

Aspects of Dynamic Recrystallization in Cobalt at High Temperatures

R. KAPOOR, B. PAUL, S. RAVEENDRA, I. SAMAJDAR, and J.K. CHAKRAVARTTY

Deformation behavior of cobalt in the fcc phase was studied over a wide range of strain rates (0.001 to 1 s^{-1}) and temperatures ($600 \text{ }^\circ\text{C}$ to $950 \text{ }^\circ\text{C}$). At the lower temperatures and higher strain rates, a single peak in flow stress followed by softening to steady state was observed, whereas at higher temperatures and lower strain rates, an oscillatory flow stress behavior finally converging to a steady state was observed. Both these represent typical flow stress responses during dynamic recrystallization (DRX). The critical condition for the initiation of DRX was determined by the inflection point in the work-hardening *vs* stress plot. This critical condition in terms of the work done was found to increase with temperature-compensated strain rate. Electron backscattered diffraction (EBSD) revealed that, on quenching after deformation, a certain fraction of the fcc phase was always retained, the extent of retention being higher for smaller grain sizes. Misorientation measurements across boundaries revealed a significant amount of twins in the retained fcc phase. The grain average misorientation (GAM), signifying the misorientation within grains, was found to be inversely related to the twin boundary fractions in the fcc phase.

DOI: 10.1007/s11661-009-9782-8

© The Minerals, Metals & Materials Society and ASM International 2009

I. INTRODUCTION

DYNAMIC recrystallization (DRX) during the hot deformation of materials has been widely studied and fairly well understood (References 1 and 2 give a good account of the basics of DRX). Materials with moderate to low stacking fault energy (SFE) are expected to favor the process of DRX, *e.g.*, Cu, Cu-Al alloys,^[3-5] and stainless steels.^[6-10] The typical mechanical response of a material during DRX is a peak in the stress-strain curve followed by either a gradual decrease in the stress to a steady-state value or the occurrence of multiple peaks (oscillations) in stress finally leading to a steady state. It is customary to identify certain parameters during DRX such as peak stress σ_p , corresponding strain ε_p , critical strain ε_c , critical stress σ_c at the start of DRX, steady-state stress σ_s , and steady-state grain size d_s , and to relate these with the deformation conditions of strain rate $\dot{\varepsilon}$ and temperature T through the temperature-compensated strain rate, also called the Zener-Hollomon parameter $Z \equiv \dot{\varepsilon} \exp(Q/RT)$, where Q is the activation energy of the process.^[1,2] Although the concept of a critical strain is very often used to characterize the start of DRX, it was argued by Wray^[11] that, since the driving force for DRX

depends on the stored energy in the material, the criteria for the start of DRX should be the amount of the stored energy (a function of work done on material during deformation) prior to the start of DRX, rather than the strain. Later the concepts of irreversible thermodynamics, again based on the stored energy criteria, were used by Poliak and Jonas^[6] to identify the critical condition for the initiation of DRX. Here, for the initiation of DRX, the local stored energy should attain a maximum and the rate of dissipation should reduce to a minimum. Using this and the hardness parameter of Hart,^[12] the critical condition for DRX was identified as the point of inflection in the θ *vs* σ plot, where θ is the work-hardening rate $\partial\sigma/\partial\varepsilon$. This implies a minimum in $-(\partial\theta/\partial\sigma)$. During DRX, inflections in the θ - σ curve have been observed earlier,^[13] but no specific explanation for this was provided. A clearer physical picture was given by Gottstein *et al.*,^[14] in which they used a three-internal-variable model (dislocation density of three kinds: mobile, stored in cell interiors, and stored in cell walls) and showed the θ - σ plot to have an inflection. Their interpretation was related to the various stages of hardening: III, IV, and V. During stage III, θ decreases with increasing σ , but before θ reaches zero, stage IV hardening takes over in which θ reduces only marginally with increasing σ . Finally, due to microstructural changes, θ rapidly falls to zero (stage V), resulting in a steady state of σ . It is between these stages IV and V that the inflection in the θ - σ curve occurs. Gottstein *et al.*^[14] cautioned that the presence of an inflection point is necessary but is not a sufficient criterion for DRX. Further, they argued against the use of ε_c as a fundamental measure of DRX initiation, since ε_c is only a value of strain where the critical conditions are met and does

R. KAPOOR, B. PAUL, and J.K. CHAKRAVARTTY, Scientific Officers, are with the Materials Group, Bhabha Atomic Research Centre, Mumbai-400 085, India. S. RAVEENDRA, Graduate Student, and I. SAMAJDAR, Professor, are with the Department of Metallurgical Engineering and Materials Science, Indian Institute of Technology Bombay, Powai, Mumbai-400 076, India. Contact e-mail: rk Kapoor@barc.gov.in

Manuscript submitted October 21, 2008.

Article published online February 20, 2009

not have a physical basis; instead, they preferred the use of σ_c . In materials that show DRX, this θ - σ inflection point has been frequently used to identify its start.^[8–10,15,16]

Apart from the critical condition for DRX, the subsequent σ - ε behavior is also of interest in the understanding of microstructural evolution. It has been observed that the recrystallized steady-state grain size d_s is an exclusive function of Z , and in turn σ_s ; d_s decreases with increasing Z and σ_s .^[3] Further, it has been shown that d_s does not depend on the initial grain size d_0 .^[17] However, the shape of the σ - ε curve depends on d_0 in addition to the deformation conditions of $\dot{\varepsilon}$ and T (and, hence, on d_s). It has been well illustrated by Sakai and Jonas^[2] that, when $d_0 > 2d_s$ (implying grain refinement), the stress-strain curve shows a single peak, and when $d_0 < d_s$ (implying grain coarsening), multiple peaks are seen. The role of twins during DRX in fcc materials has also been emphasized by many researchers.^[18–24] Many of these studies have shown that the region near the DRX front has a higher fraction of twins as compared to the interior of the DRX region. It is thought that twin formation is an important mechanism of nucleation during DRX.

Most of the DRX studies in low SFE fcc materials have concentrated on Cu and austenitic stainless steels. An interesting fcc material not so commonly studied is the high-temperature fcc phase of cobalt. The equilibrium transformation temperature of Co from hcp to fcc is about 430 °C, with a low free energy change of ~ 350 J/mol.^[25] This makes the reaction sluggish, and on quenching, some of the high-temperature fcc phase is retained, while the rest undergoes a fcc to hcp martensitic transformation.^[26,27] The fraction of retained fcc phase has been seen to depend on the existing grain size before quenching;^[28–30] the smaller the grain size, the higher the retention of fcc phase. The high-temperature fcc phase of Co has a low SFE of about 18×10^{-3} J/m²^[31] and, hence, is likely to experience DRX. Early work on the hot deformation of cobalt was carried out in compression, tension, and creep.^[32–34] In one study,^[32] mild oscillatory behavior in σ - ε curves was observed during compression of Co in the 900 °C to 1200 °C and 3 to 20 s⁻¹ range, but DRX was not explicitly mentioned.

A recent study by the present authors^[35] on the hot deformation of wrought Co in the fcc phase clearly demonstrated the occurrence of DRX. Here, examples of the flow stress behavior for both single and multiple peaks were presented, the strain rate sensitivity mapped out, and the kinetic analysis carried out. Because DRX is the primary mechanism during the hot deformation of Co, it is essential that it be studied in detail. The knowledge of the relation between microstructure, stress, and testing conditions thus obtained could be used in the control of Co microstructure during hot deformation. With this in view, the present article is an extension of the earlier work. Here, the critical condition for DRX is determined; the microstructural characterization using electron backscattered diffraction (EBSD) carried out; and the deformation conditions correlated with the stress response, the microstructure, and the retained fcc phase.

II. EXPERIMENTS

Cobalt used in this study was in the wrought condition of 6-mm-diameter rod with the following composition in weight percent: 0.05Ni, 0.015Fe, 0.005Cu, 0.03C, and 99.85Co. The as-received microstructure was essentially equiaxed with an average grain size of 10 μ m. Samples of 5-mm diameter and 7-mm height were tested in compression at temperatures between 600 °C and 950 °C (corresponding to 0.5 to 0.7 of melting temperature T_m) and true strain rates $\dot{\varepsilon}$ ranging from 10⁻³ to 1 s⁻¹. The velocity of ram was programmed to decrease with time so as to achieve a constant true strain rate. Refer to Reference 35 for the experimental procedure and early results. Alumina push rods were used for compression with hexagonal boron nitride as a lubricant. The furnace chamber was flushed with Ar to prevent excessive oxidation at high temperatures. The sample temperature was monitored by a thermocouple touching the sample surface. Immediately after the test, the sample was removed from the furnace and quenched in water. From the data of force F and displacement d , the true stress $\sigma = F(1 - e)/A_0$ and true strain $\varepsilon_{\text{tot}} = -\ln(1 - e)$ were obtained, where e is the engineering strain and A_0 is the initial cross-sectional area of sample. The plastic true strain ε was obtained by subtracting the combined (machine and sample) elastic strain from ε_{tot} as $\varepsilon = \varepsilon_{\text{tot}} - \sigma/E$, where E is the effective modulus of machine and sample. The samples were sectioned longitudinally and electropolished using 90 pct glacial acetic acid and 10 pct perchloric acid as electrolyte at 20 V and -25 °C in Struers LectroPol 5 electropolishing equipment. The EBSD measurements were made on an FEI Quanta-200 HV scanning electron microscope with a TexSEM Laboratories (TSL) orientation-imaging microscopy (OIM) EBSD system. In each sample, an area of at least 600 \times 600 μ m² was scanned with a step size of 0.5 μ m. Beam and video conditions were kept identical between the scans. For accurate phase identification (*i.e.*, distinguishing between cubic and hexagonal phases of cobalt), a minimum of 4 Kikuchi bands were taken. Grains were identified from the presence of a continuous boundary of above 5 deg misorientation. Misorientations that develop during plastic deformation are often used to characterize the deformed microstructure. In the present study, the grain average misorientation (GAM), representing the average misorientation between neighboring measurement points within each grain, was determined using EBSD.

III. RESULTS AND ANALYSIS

A. Stress-Strain Behavior

Figure 1 shows the flow stress behavior at different strain rates and temperatures. From this, the following important observations can be made. Two types of σ - ε behaviors are seen: (1) where the flow stress work hardens to a single peak and then shows a gradual drop, finally reaching a steady-state value; and (2) where the flow stress work hardens to a peak, and then shows an oscillatory behavior, with the oscillations decreasing in amplitude

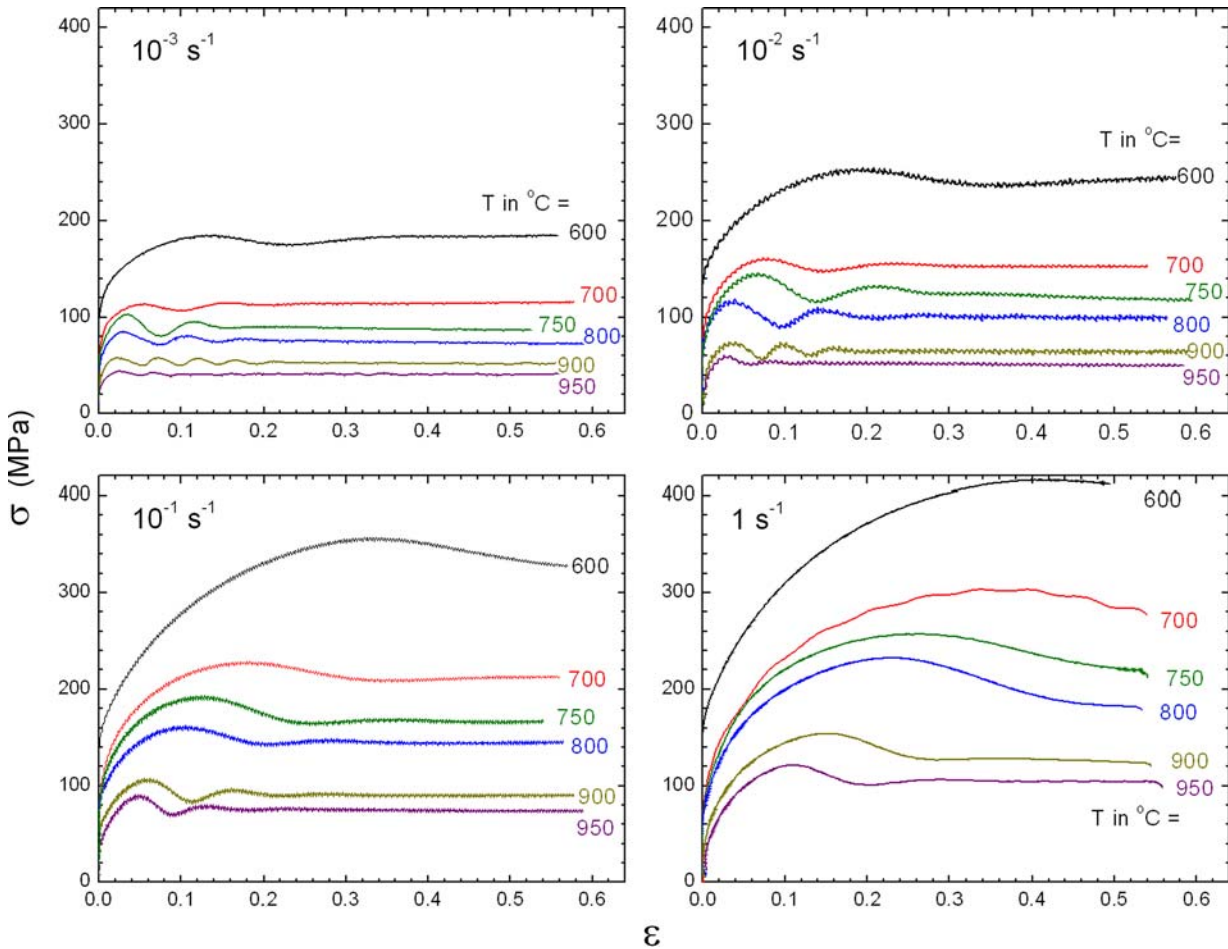


Fig. 1—True stress vs plastic true strain plots for Co at different temperatures and strain rates.

and the stress, finally converging to a steady-state value. With increasing temperature and decreasing strain rate, the following trends are observed:

- (1) the steady-state stress decreases,
- (2) the strain to the first peak stress decreases and the strain per oscillations reduce, and
- (3) multiple peaks in the flow stress are more likely to occur.

B. Critical Condition for DRX

The critical condition for the initiation of DRX was determined from the inflection point in the θ vs σ plot, as shown in Figure 2. The value of θ was calculated by taking the derivative of the σ - ϵ curves. For this, the interpolated stress values at sufficiently far apart strain intervals were taken so as to avoid introducing noise during the process of taking the derivative. The value of θ for the i th point was calculated as

$$\theta_i = \frac{\sigma_{i+1} - \sigma_{i-1}}{\epsilon_{i+1} - \epsilon_{i-1}} \quad [1]$$

The inflection points of these curves were obtained from the minima of the $d\theta/d\sigma$ curves; this derivative was also calculated by the method similar to that shown in

Eq. [1]. Figure 2 also shows the corresponding $d\theta/d\sigma$ - σ plots as insets. From these curves, σ_c was determined, and in conjunction with the σ - ϵ curves, the corresponding critical strain ϵ_c was determined. The work done per unit mass on the sample up to the critical condition of DRX (W_c) and to the peak stress (W_p) were determined following Reference 11 as

$$W_c = \frac{1}{\rho} \int_0^{\epsilon_c} \sigma d\epsilon \quad \text{and} \quad W_p = \frac{1}{\rho} \int_0^{\epsilon_p} \sigma d\epsilon \quad [2a, b]$$

where ρ is the mass density of the material. The preceding analysis showed that $\epsilon_c \approx 0.5 \epsilon_p$ and $W_c = 0.35 W_p$, as seen in Figure 3.

C. Strain Rate and Temperature Effect

Figure 4 shows an increase of steady-state stress σ_s with plastic true strain rate at all the temperatures of testing. The slope of this is the strain rate sensitivity $m = \partial \ln \sigma / \partial \ln \dot{\epsilon}$, which is an important deformation parameter. Higher values of m result in delayed strain localization during working. The magnitude of m also helps in the identification of deformation mechanisms.

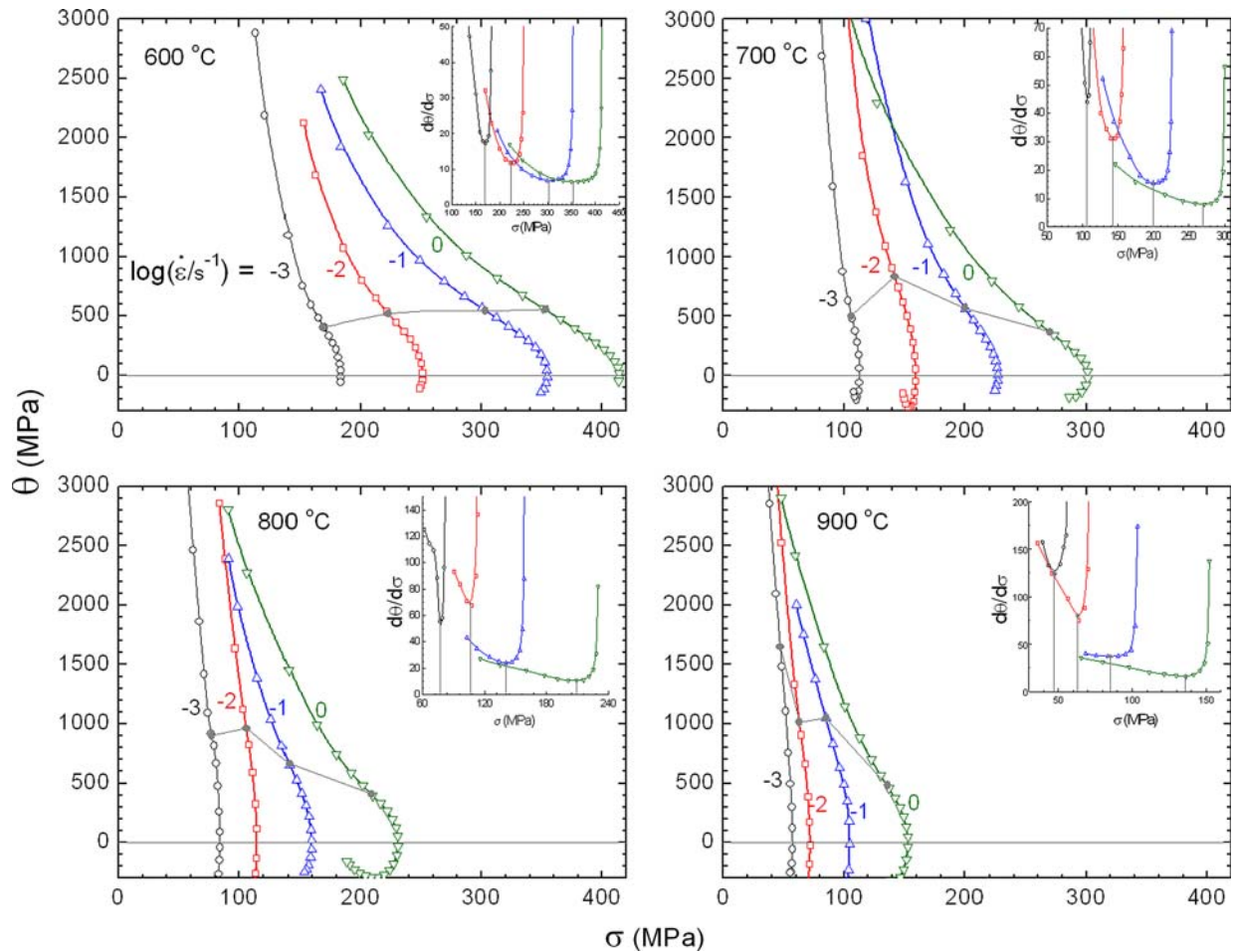


Fig. 2—Strain hardening vs stress plots for Co, as obtained from Fig. 1. The log values of $\dot{\epsilon}$ are indicated on each curve. The loci of inflection points are marked with gray dots connected with a line. Insets show the $d\theta/d\sigma$ vs σ plots used to identify the inflection points. The gray vertical lines in the inset indicate the minima corresponding to the inflection point in the θ - σ curves.

In an earlier analysis of this work,^[35] m was calculated and mapped on the $\dot{\epsilon}$ - T axis to identify regimes of high m so as to optimize hot workability. It was seen that m varied from about 0.1 to 0.15. The σ_s normalized by shear modulus μ was collapsed on one curve using the temperature-compensated strain rate $Z \equiv \dot{\epsilon} \exp(Q/RT)$ (Figure 4 of Reference 35). Here, Z was found to increase with σ_s/μ in a power-law relation:

$$\dot{\epsilon} = A(\sigma_s/\mu)^n \exp(-Q/RT), \text{ or } Z = A(\sigma_s/\mu)^n \quad [3a, b]$$

where n is the stress exponent, and A is a constant. From the preceding fit, $Q = 254$ kJ/mol and $n = 7.66$ were obtained using Z , which was calculated and plotted against the critical work done for initiation of DRX, W_c . As seen in Figure 5, W_c increases in a power-law behavior with Z for most of the conditions where multiple peaks occur.

D. Retention of Fcc Phase

From the EBSD measurements, amounts (*i.e.*, area fraction) of the fcc and hcp phases were estimated for both the deformed and undeformed samples (those

samples that were held at the required testing temperature and quenched without deformation). In all samples, a certain fraction of the fcc phase was always retained after quenching to ambient temperature. It was seen that, with increasing Z , the area fraction of the retained fcc phase increased (Figure 6(a)). From EBSD analysis, the steady-state grain size distributions for both the fcc and hcp phases were determined. The combined hcp and retained fcc grain size distribution, as measured through EBSD at room temperature, represents the overall steady-state grain size prior to quenching.*

*The fcc to hcp transformation is martensitic in nature, and the martensite plates that form within the prior fcc grains have a low misorientation between themselves as compared to that across the prior fcc grain boundaries, and are hence not revealed as clearly. Thus, the hcp grains obtained on quenching represent the prior fcc grains in terms of grain size.

It is seen that the area fraction of the retained fcc phase is inversely related to the overall steady-state grain size (Figure 6(b)). This implies that smaller fcc grains have a higher probability of being retained on quenching as

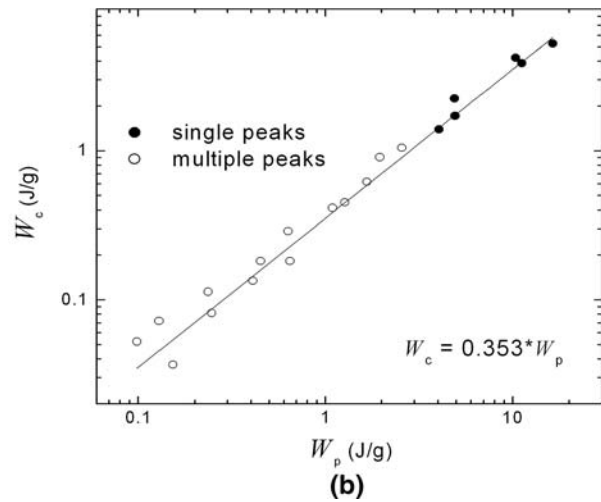
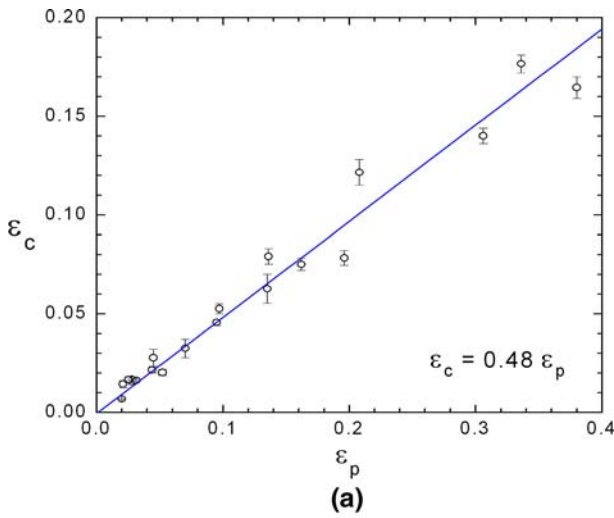


Fig. 3—Relation between (a) strain at peak stress and critical strain and (b) work done to peak stress and to critical value.

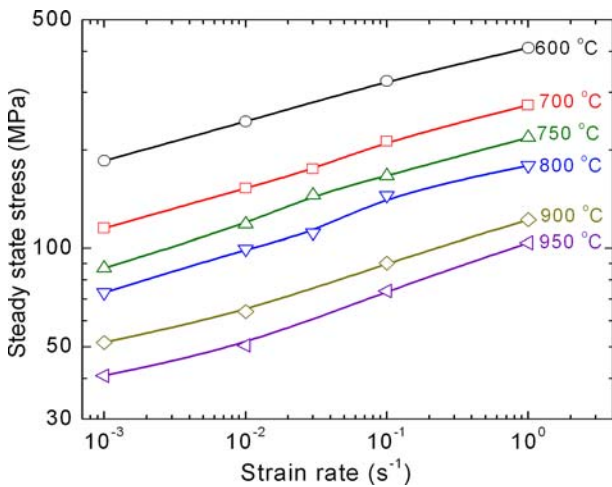


Fig. 4—Steady-state stress vs strain rate for Co deformed at different temperatures.

compared to larger ones. An example of some typical features of the retained fcc phase after deformation and quenching are shown in Figure 7. The percentage

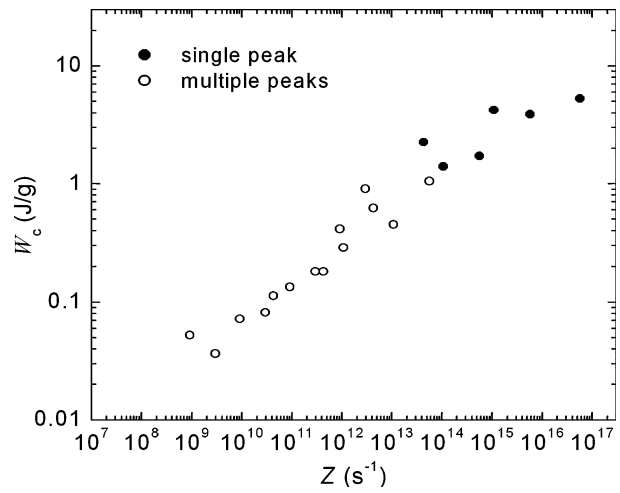


Fig. 5—Variation of critical work done, W_c , for initiation of DRX given by Eq. [2a] as a function of Z . The conditions of single and multiple peaks are indicated.

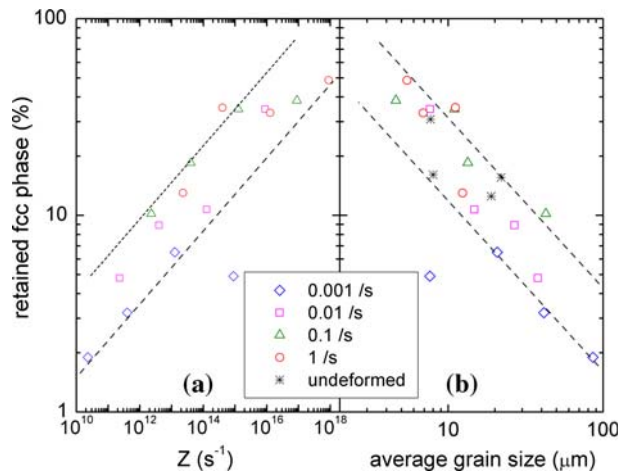


Fig. 6—Amount of retained fcc phase as a function of both Z and the average of the overall grain size. The dotted lines represent the trend and band of scatter.

retained fcc phase of the deformed samples are mentioned in the figure caption. The microstructure shows straight boundaries with distinctive appearance of twins. The fcc $\Sigma 3$ twins (Σ representing CSL or coincident site lattice) are 60 deg $\langle 111 \rangle$ boundaries. Misorientation profiles, for boundary misorientations >5 deg, show a large fraction of grains having a misorientation of ~ 60 deg, as shown in Figure 8 for 700 °C (also seen at other temperatures). This, on the other hand, supports the qualitative observation, on possible twin presence, made in Figure 7. Figure 9 plots the fraction of $\Sigma 3$ boundaries at different temperatures and working conditions. The deformed samples, in general, show higher fractions of $\Sigma 3$ twin boundaries.

IV. DISCUSSION

This work brings out the classical effect of DRX on flow stress softening, both with and without oscillations,

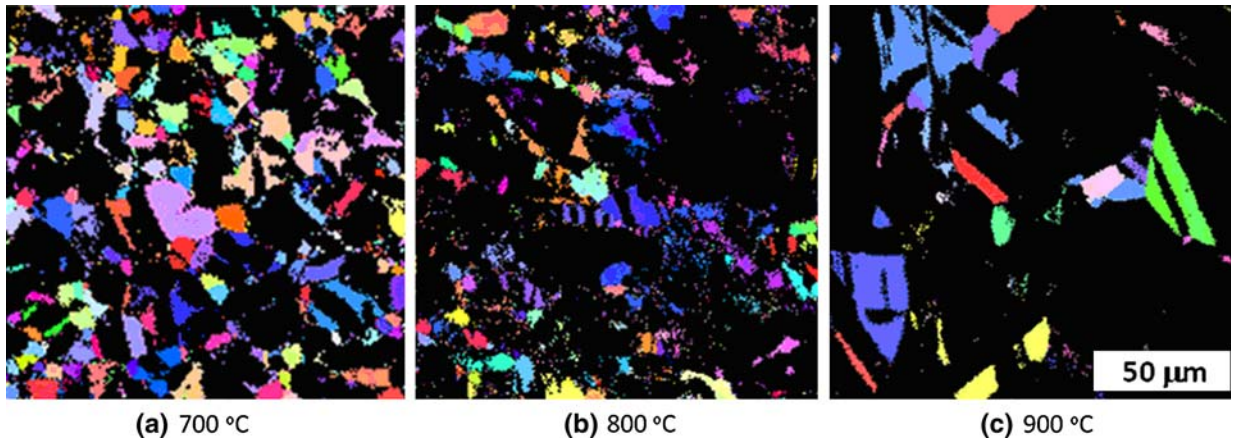


Fig. 7—EBSD image of quenched samples after testing at 0.1 s^{-1} and at the indicated temperatures. The light areas represent the retained fcc phase, and the black areas represent the hcp phase. For this testing condition, the amount of retained fcc is 35 pct for 700 °C, 19 pct for 800 °C, and 10 pct for 900 °C.

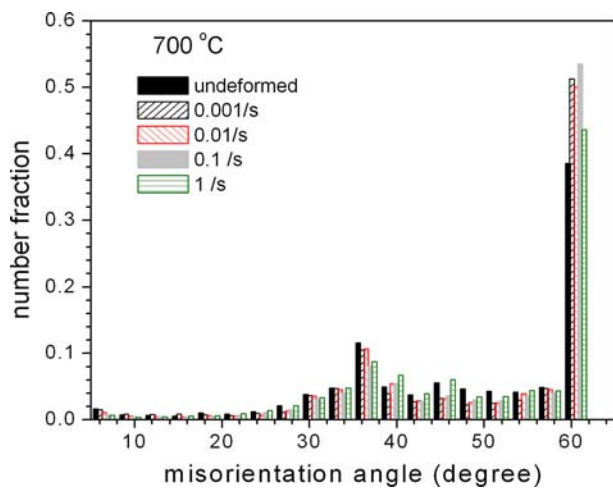


Fig. 8—Histogram showing the misorientation angle distribution at 700 °C and different testing conditions including the undeformed condition.

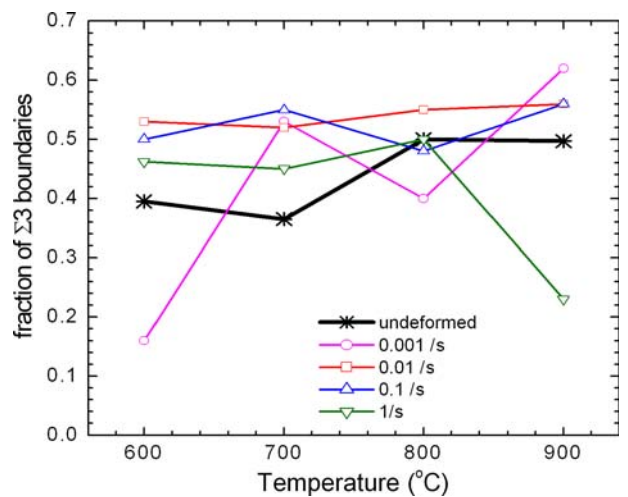


Fig. 9—Fraction of CSL $\Sigma 3$ boundaries as a function of testing temperature at various strain rates. Also shown for comparison are the values for undeformed Co.

followed by a steady-state behavior. A clear trend emerges with increasing temperature and decreasing strain rate: the peak stress is achieved at a lower strain and the number of oscillations before steady state is increased. This is clear evidence of the occurrence of DRX in fcc phase Co through most of the testing conditions.

A. Critical Condition for DRX

The identification of a critical condition for the initiation of DRX is important. The direct method of the determination of such a condition is through microstructural observations, where sample deformation is interrupted at intermittent strains and features of DRX are noted (e.g., References 5, 22, and 36). It is relatively simpler to adopt this method while dealing with single-phase materials, which do not undergo transformations on cooling. However, for materials

undergoing transformations from the temperature of deformation to ambient, as in Co, the identification of initiation of DRX can get difficult. The indirect technique of determining the critical condition of DRX through the inflection in θ - σ curve resulted in $\epsilon_c = 0.5 \epsilon_p$ and $W_c = 0.35 W_p$. Previous studies that have used this θ - σ analysis have also obtained a ratio of ϵ_c/ϵ_p close to 0.5 in steels^[8,10,16] and a Mg alloy.^[15] However, a similar relation between W_c and W_p has not been reported earlier. It was also seen that W_c increases as a power law with increasing temperature-compensated strain rate Z (Figure 5). Since Z and σ_s are related (through Eq. [3]), this observation implies that W_c would increase with σ_s also through a power law.

B. Regions of Single and Multiple Peaks

Sakai and Jonas^[2] in their review article elaborately explained the conditions where single and multiple

peaks occur. It was shown by them that the critical Z (referred to as Z_c), which indicates a changeover from single to multiple peaks, is inversely related to d_0 . It is also known that, during DRX, Z is inversely related to d_s .^[1,3,17,37] Although Z - d_s and Z_c - d_0 curves have similar behavior, the Z_c - d_0 curve was shown to be parallel to and higher than the Z - d_s curve. In fact, for an austenitic steel, the Z_c - d_0 curve matched the Z - $2d_s$ curve.** All

**For details, see Fig. 15 of Ref. 2, where Z_c - d_0 and Z - $2d_s$ curves were plotted together on a log-linear scale. In the present Fig. 10, a log-log scale was chosen to clearly bring out the inverse behavior of Z vs grain size.

conditions to the right of the Z_c - d_0 curve represent the single peak regime, and all conditions to the left represent the multiple peak regime. When the initial grain size is to the right of the Z - $2d_s$ curve, it would need to decrease to reach the curve, and when on the left of the curve, it would need to increase to reach the curve (here, Z is constant, *i.e.*, at fixed testing condition). This finding implies that the right side of the curve, which represents the single peak regime, results in grain refinement, whereas the left side of the curve, which represents the multiple peaks regime, results in grain coarsening.

A similar analysis was carried out for the present Co results for which the average overall grain sizes just before and after deformation, representing d_0 and d_s , respectively, were obtained through EBSD. Table I lists the initial grain size at each temperature as well as the ratio d_s/d_0 at each testing condition and mentions whether the σ - ε curve shows single or multiple peaks. Further, for this analysis, the condition for changeover from single to multiple peaks Z (Z_c) needs to be estimated. The value of Z_c was obtained from $\dot{\varepsilon}_c \exp(Q/RT)$, where $\dot{\varepsilon}_c$ is the critical strain rate, indicating the transition from single to multiple peaks. The value of $\dot{\varepsilon}_c$ was estimated as the average of the log of the two strain rates, one where a single peak occurs and the next lower one where multiple peaks occur at the given temperature T . For example, referring to Table I, at 600 °C, $\dot{\varepsilon}_c$ would lie between 0.01 and 0.001 s⁻¹ and was taken as $(0.01 \times 0.001)^{0.5}$ s⁻¹; at 700 °C, $\dot{\varepsilon}_c$ would lie between 0.1 and 0.01 s⁻¹ and was taken as $(0.1 \times 0.01)^{0.5}$ s⁻¹. Figure 10 shows the Z - d_s plot for

Table I. Initial Grain Sizes (d_0) Prior to Testing at Each Temperature and the Ratio of Final to Initial Grain Size at Each Testing Condition Are Listed; Also Indicated Are Those Deformation Conditions Where a Single Peak (S) or Multiple Peaks (M) Occur

$\dot{\varepsilon}$	T			
	600 °C	700 °C	800 °C	900 °C
1 s ⁻¹	0.8 S	1.1 S	0.7 S	0.6 S
0.1 s ⁻¹	0.7 S	1.8 S	0.8 M	2.1 M
0.01 s ⁻¹	1 S	2.2 M	1.6 M	2 M
0.001 s ⁻¹	1.2 M	3.2 M	2.4 M	4.3 M
d_0 at each T	7.5 μ m	8 μ m	19 μ m	22 μ m

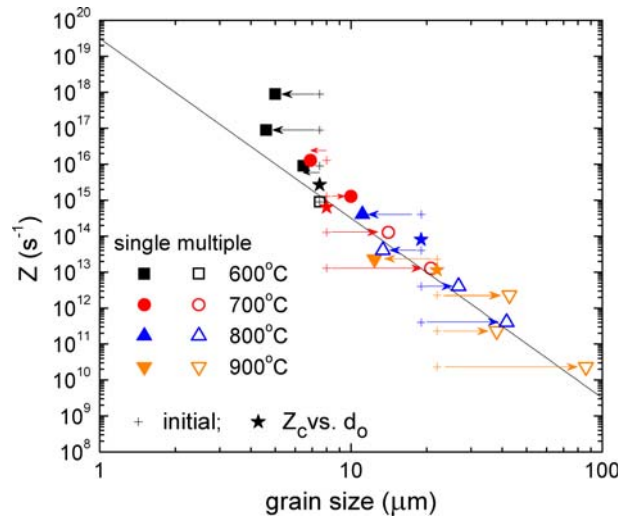


Fig. 10—Temperature-compensated strain rate vs grain size for Co at different temperatures. The plus symbol represents the initial grain size, and the arrows connect these to the steady-state grain size represented by shapes. The star signs are the estimated value of Z_c , which represent the transition from multiple to single peak. The solid line is the trend line of the Z vs grain size behavior at steady state.

the present Co data from which the following observations are striking.

- (1) The term Z is inversely related to d_s over the entire testing range.
- (2) The initial grain sizes at the testing temperature (+ symbols) and the final steady-state values (round symbols) are shown in the figure. The arrows connect the initial grain sizes to the final ones. Thus, arrows pointing right imply grain coarsening, whereas arrows pointing left imply grain refinement. Grain coarsening occurs when $d_0 < d_s$, and grain refinement occurs when $d_0 > d_s$.
- (3) Most multiple peaks occur (hollow symbols) during coarsening, and most single peak behavior occurs (filled symbols) during refinement.
- (4) The Z_c - d_0 data are also plotted in Fig. 10 as solid stars. It is seen that the Z_c - d_0 data lie on the Z - d_s curve.

These observations match earlier studies; there is only a small difference in that, here, Z_c - d_0 matches Z - d_s , rather than Z - $2d_s$, as mentioned in Reference 2. However, some results in steels undergoing DRX^[38] also showed that Z_c - d_0 matches Z - d_s as in this study.

The relation between multiple peaks and grain coarsening, and single peak and grain refinement, was confirmed by performing strain rate change tests. These tests also check for the strain rate history dependence of the steady-state stress (and, hence, indirectly d_s). In one such test at 900 °C, the strain rate was increased from 0.01 to 0.1 s⁻¹, then decreased to 0.001 s⁻¹, and increased back to 0.01 s⁻¹, as seen in Figure 11. It is seen that, when the strain rate is increased from 0.01 to 0.1 s⁻¹, a single peak occurs followed by a steady state, whereas the straight test at 0.1 s⁻¹ showed multiple peaks. This is consistent with the regimes of the Z - d_s plot of single and multiple peaks, as explained previously. When deformed

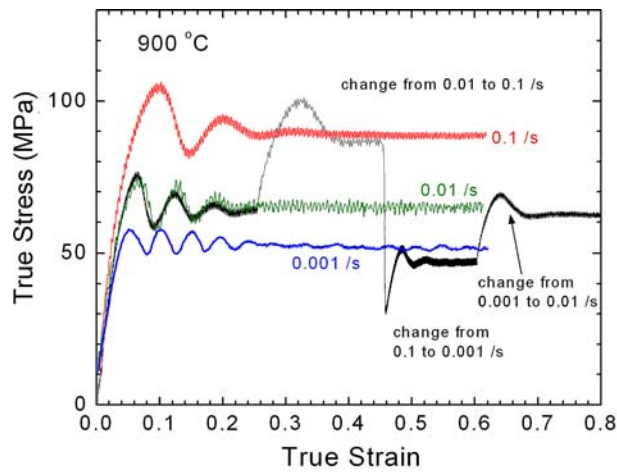


Fig. 11—Strain rate change tests at 900 °C. Shown here are three tests at constant strain rates of 0.001, 0.01, and 0.1 s⁻¹ and one strain rate change test from 0.01 to 0.1 to 0.001 to 0.01 s⁻¹.

Table II. Average Grain Sizes in Microns of the Retained Fcc Phase at Different Temperatures and Strain Rates

$\dot{\epsilon}$	T			
	600 °C	700 °C	800 °C	900 °C
1 s ⁻¹	5.1	4.8	8	7
0.1 s ⁻¹	3.5	8	6.6	13
0.01 s ⁻¹	4.5	6	8.2	8.8
0.001 s ⁻¹	2.7	5.7	5.8	7.2

at 900 °C and 0.01 s⁻¹, a steady-state grain size is achieved, which would tend to decrease when the strain rate is increased to 0.1 s⁻¹ (a higher $\dot{\epsilon}$ implies higher σ_s and, hence, lower d_s). For this decrease in grain size, the flow behavior shows a single peak, although the initial flow behavior at 0.1 s⁻¹ showed multiple peaks. A decrease in $\dot{\epsilon}$ from 0.1 to 0.001 s⁻¹ results in a drop in flow stress with weak multiple peaks to a steady-state level close to that of the straight test at 0.001 s⁻¹. This change from higher to lower strain rate would tend to increase the grain size (in accordance with a decrease in flow stress), which would result in multiple oscillations in the flow stress curve. Last, when the strain rate is again increased to 0.01 s⁻¹, the grain size tends to decrease (as stress increases), hence showing a single peak, although the straight test at 0.01 s⁻¹ showed multiple peaks. This strain rate change test confirms the relationship between single peak and grain refinement, and multiple peaks and grain coarsening. Further, there appears practically no history dependence of the steady-state flow stress on deformation conditions, as evidenced by the matching of the steady-state stress after strain rate changes.

C. Retained Fcc Phase and Its Misorientation

The fcc to hcp transformation on cooling has a low free energy change and, hence, is sluggish. This results in a certain fraction of the fcc phase being retained on quenching from high temperatures. In the present study, a certain amount of retained fcc phase is always present

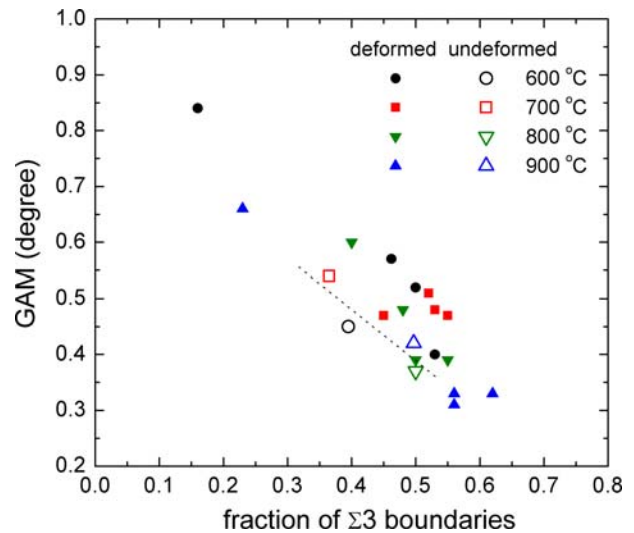


Fig. 12—GAM as a function of the fraction of $\Sigma 3$ boundaries for different deformation conditions. Also shown are values for the undeformed condition. The dashed line shows the trend of the undeformed samples (hollow symbols).

when observed at room temperature. From EBSD measurements, the grain size distribution and the area fraction of both the hcp and fcc phases were obtained for each sample. As seen in Table II, the average grain size of the retained fcc phase remains around or below 10 μm , although the overall grain size for the same testing condition is much higher (Table I). This suggests that it is only the small fcc grains that are retained; the larger ones transform to hcp on quenching. This is in agreement with Figure 6(b), where it was seen that, with decreasing overall grain size, the fraction of retained fcc increased. The inverse relation between d_s and Z (Figure 10) supports the conclusion that the overall grain size measured after quenching represents the original fcc grain size just prior to quenching.

The average point-to-point misorientation or the GAM values were determined within a grain. This is an important parameter, which signifies the extent of in-grain misorientation development (an important feature of plastic deformation) within a grain. For example, a statically recrystallized grain would have a very low GAM (a value which may represent measurement uncertainty), while a deformed grain would be expected to show an increased GAM. Grain average misorientation has been used by researchers to measure intragrain misorientations (*e.g.*, References 39 through 41; in particular, Reference 39 shows the increase of GAM with strain in a bcc steel).

The GAM calculated for all conditions was correlated to the fraction of $\Sigma 3$ twin boundaries $f_{\Sigma 3}$, as shown in Figure 12. An inverse trend is seen here; the higher the $f_{\Sigma 3}$, the lower the GAM. Although at first glance the data may appear to have a large scatter, if looked at with each temperature, the trend is clearer. The GAM- $f_{\Sigma 3}$ trend for the undeformed Co (dashed line in Figure 12) is lower than that for the 600 °C and 700 °C deformed samples. At 800 °C, the GAM- $f_{\Sigma 3}$ trend is higher than that for the undeformed samples but

not as much as that of the 600 °C and 700 °C deformed samples. At 900 °C, the GAM- $f_{\Sigma 3}$ trend matches that of the undeformed conditions. These observations suggest that deformation at 600 °C and 700 °C still contains defects that have not recovered or been consumed by the recrystallization process. At 800 °C, this is less so, and at 900 °C, the extent of recovery after testing and before quenching is enough to reduce the hardening to those of the undeformed levels. The marginally higher GAM for the deformed structure may suggest the occurrence of DRX.

It was observed that a high $f_{\Sigma 3}$ exists at most testing conditions (Figures 8 and 9). Twins are known to play an important role during the nucleation of DRX. It has been shown in Cu^[5] that twins form at triple junctions at strains lower than the estimated critical strain. At low strains, grain boundaries start forming serrations, which result in nucleation of new grains, some of which are twins.^[22] It has been argued that the formation of twins is due to grain boundary migration,^[20–22] as in the case of annealing twins,^[42] and not due to slip activity within grains.^[22] In the present study, a high $f_{\Sigma 3}$ exists in the undeformed structure to start with. These would be annealing twins formed during the process of holding at the high temperature prior to testing. On deformation, $f_{\Sigma 3}$ increases by a small amount, suggesting that these twins have been nucleated during DRX. The lower GAM associated with the higher twin fraction indicates that the $\Sigma 3$ twins are relatively free of deformation. This implies that the twins are either freshly nucleated or do not deform significantly as compared to the original grains.

V. CONCLUSIONS

1. High-temperature deformation of Co in the fcc phase shows a flow behavior typical of the process of DRX, *i.e.*, the presence of a single peak followed by softening at higher Z and multiple peaks converging to steady state at lower Z .
2. The critical condition for the initiation of DRX, as obtained through the θ - σ inflection point, was presented in terms of the work done during deformation up to the critical strain. The work done to the initiation of DRX was found to be about one third of the work done to peak stress. Also, this critical work done, W_c , was found to increase with increasing Z through a power law.
3. It was shown that, during DRX, the occurrence of multiple peaks in Co was related to the process of grain growth, whereas the occurrence of single peak was related to the process of grain refinement. Also, the steady-state stress was found to depend exclusively on the current deformation conditions and appeared unaffected by previous deformation history, as confirmed through strain rate change tests.
4. Retention of the fcc phase after quenching to room temperature was observed in all samples. The fraction of retained fcc was found to increase with increasing Z and decreasing initial overall grain

size. This implies that the finer the fcc grains, the higher the likelihood of retention during quenching.

5. A large fraction of the retained fcc grain boundaries were of $\Sigma 3$ twins. Although the undeformed samples did contain a high fraction of twins, these increased marginally on deformation. Samples with a larger fraction of twins also showed a lower GAM, suggesting that the observed twins are either freshly nucleated or deform less than the untwinned grains.

REFERENCES

1. H.J. McQueen and J.J. Jonas: *Treatise Mater. Sci. Technol.*, 1975, vol. 6, pp. 393–493.
2. T. Sakai and J.J. Jonas: *Acta Metall.*, 1984, vol. 32, pp. 189–209.
3. M. Ueki, S. Horie, and T. Nakamura: *Mater. Sci. Technol.*, 1987, vol. 3, pp. 329–37.
4. W. Gao, A. Belyakov, H. Miura, and T. Sakai: *Mater. Sci. Eng. A*, 1999, vol. 265, pp. 233–39.
5. M. Miura, T. Sakai, H. Hamaji, and J.J. Jonas: *Scripta Mater.*, 2004, vol. 50, pp. 65–69.
6. E.I. Poliak and J.J. Jonas: *Acta Mater.*, 1996, vol. 44, pp. 127–36.
7. A. Belyakov, K. Tsuzaki, H. Miura, and T. Sakai: *Acta Mater.*, 2003, vol. 51, pp. 847–61.
8. E.I. Poliak and J.J. Jonas: *ISIS Int.*, 2003, vol. 43, pp. 684–91.
9. G. Gottstein, M. Frommert, M. Goerdeler, and N. Schäfer: *Mater. Sci. Eng. A*, 2004, vols. 387–389, pp. 604–08.
10. A. Dehghan-Manshadi, M.R. Barnett, and P.D. Hodgson: *Mater. Sci. Eng. A*, 2008, vol. 485, pp. 664–72.
11. P.J. Wray: *Metall. Trans. A*, 1975, vol. 6A, pp. 1197–1203.
12. E.W. Hart: *Acta Metall.*, 1970, vol. 18, pp. 599–610.
13. N.D. Ryan and H.J. McQueen: *Can. Met. Q.*, 1990, vol. 29, pp. 147–62.
14. G. Gottstein, E. Brünger, M. Frommert, M. Goerdeler, and M. Zeng: *Z. Metallkd.*, 2003, vol. 94, pp. 628–35.
15. L. Liu, H. Zhou, Q. Wang, Y. Zhu, and W. Ding: *J. Mater. Online*, DOI 10.2240/azojomo0211.
16. Z. Zhang, Y. Liu, X. Liang, and Y. She: *Mater. Sci. Eng. A*, 2008, vol. 474, pp. 254–60.
17. J.P. Sah, G.J. Richardson, and C.M. Sellars: *Met. Sci.*, 1974, vol. 8, pp. 325–31.
18. G. Gottstein, D. Zabarjadi, and H. Mecking: *Met. Sci.*, 1979, vol. 13, pp. 223–27.
19. D. Ponge and G. Gottstein: *Acta Mater.*, 1998, vol. 46, pp. 69–80.
20. E. Brünger, X. Wang, and G. Gottstein: *Scripta Mater.*, 1998, vol. 38, pp. 1843–49.
21. X. Wang, E. Brünger, and G. Gottstein: *Scripta Mater.*, 2002, vol. 46, pp. 875–80.
22. H. Miura, T. Sakai, R. Mogawa, and G. Gottstein: *Scripta Mater.*, 2004, vol. 51, pp. 671–75.
23. Y.S. Na, J.T. Yeom, N.K. Park, and J.Y. Lee: *Metall. Mater. Trans. A*, 2006, vol. 37A, pp. 41–47.
24. Y. Wang, W.S. Shao, L. Zhen, and X.M. Zhang: *Mater. Sci. Eng. A*, 2008, vol. 486, pp. 321–32.
25. W. Betteridge: *Prog. Mater. Sci.*, 1979, vol. 24, pp. 51–142.
26. C. Wen, B. Huang, Z. Chen, and Y. Rong: *Mater. Sci. Eng. A*, 2006, vols. 438–440, pp. 420–26.
27. J.C. Zhao and M.R. Notis: *Scripta Metall. Mater.*, 1995, vol. 32, pp. 1671–76.
28. E.A. Owen and D.M. Jones: *Proc. Phys. Soc.*, 1954, vol. 67B, pp. 456–66.
29. X.Q. Zhao, S. Veintemillas-Verdaguer, O. Bomati-Miguel, M.P. Morales, and H.B. Xu: *Phys. Rev. B*, 2005, vol. 71, pp. 024106-1–024106-7.
30. C. Hayzelden, K. Chattopadhyay, J.C. Barry, and B. Cantor: *Phil. Mag. A*, 1991, vol. 63, pp. 461–70.
31. T. Ericsson: *Acta Metall.*, 1966, vol. 14, pp. 853–65.
32. J.M. Jacques and L. Habraken: *Cobalt*, 1968, vol. 38, pp. 13–19.
33. H. Beckers, L. Fontains, B. Tougarinoff, and L. Habraken: *Cobalt*, 1964, vol. 25, pp. 171–86.
34. P. Feltham and T. Myers: *Phil. Mag.*, 1963, vol. 8, pp. 203–11.

35. B. Paul, R. Kapoor, J.K. Chakravarty, A.C. Bidaye, I.G. Sharma, and A.K. Suri: *Scripta Mater.*, 2008, vol. 60, pp. 104–07.
36. S. Sakui, T. Sakai, and K. Takeshi: *Trans. Iron Steel Inst. Jpn.*, 1977, vol. 17, pp. 718–25.
37. M.J. Luton and C.M. Sellars: *Acta Metall.*, 1969, vol. 17, pp. 1033–43.
38. T. Maki, K. Akasaka, and I. Tamura: in *Thermomechanical Processing of Microalloyed Austenite*, A.J. DeArdo, G.A. Ratz, and P.J. Wray, eds., American Institute of Mining Engineers, Warrendale, PA, 1982, pp. 217–52.
39. J.Y. Kang, B. Bacroix, H. Réglé, K.H. Oh, and H.C. Lee: *Acta Mater.*, 2007, vol. 55, p. 4935.
40. J.H. Cho, J.S. Cho, J.T. Moon, J. Lee, Y.H. Cho, Y.W. Kim, A.D. Rollet, and K.H. Oh: *Metall. Mater. Trans. A*, 2003, vol. 34A, pp. 1113–25.
41. S. Raveendra, S. Mishra, K.V. ManiKrishna, H. Weiland, and I. Samajdar: *Metall. Mater. Trans. A*, 2008, vol. 39A, pp. 2760–71.
42. S. Mahajan, C.S. Pande, M.A. Imam, and B.B. Rath: *Acta Mater.*, 1997, vol. 45, pp. 2633–38.